

## Article

# Rearrangement of Diferrocenyl 3,4-Thiophene Dicarboxylate

Asma Ghazzy<sup>1</sup>, Deeb Taher<sup>2,\*</sup>, Marcus Korb<sup>3</sup> , Khaled Al Khalyfeh<sup>4</sup> , Wissam Helal<sup>2</sup> , Hazem Amarne<sup>2</sup> , Tobias Rüffer<sup>5</sup>, Zakariyya Ishtaiwi<sup>6</sup>  and Heinrich Lang<sup>5,7</sup>

- <sup>1</sup> Faculty of Pharmacy, Al Ahliyya Amman University, Amman 19328, Jordan; a.alghazzy@ammanu.edu.jo  
<sup>2</sup> Department of Chemistry, The University of Jordan, Amman 11942, Jordan; wissam.helal@ju.edu.jo (W.H.); h.amarne@ju.edu.jo (H.A.)  
<sup>3</sup> School of Molecular Sciences, The University of Western Australia, Perth, WA 6009, Australia; marcus.korb@uwa.edu.au  
<sup>4</sup> Department of Chemistry, Faculty of Natural Sciences, Al-Hussein Bin Talal University, Ma'an 71111, Jordan; k.khalyfeh@ahu.edu.jo  
<sup>5</sup> Faculty of Natural Sciences, Institute of Chemistry, Technische Universität Chemnitz, Inorganic Chemistry, D-09107 Chemnitz, Germany; tobias.rueffer@chemie.tu-chemnitz.de (T.R.); heinrich.lang@chemie.tu-chemnitz.de (H.L.)  
<sup>6</sup> Department of Chemistry, Faculty of Science, Al-Balqa Applied University, Al Salt 19117, Jordan; zak1777@bau.edu.jo  
<sup>7</sup> MAIN Research Center, Technische Universität Chemnitz, Rosenbergstraße 6, D-09126 Chemnitz, Germany  
\* Correspondence: d.taher@ju.edu.jo; Tel.: +962-(0)6-535-5000 (ext. 22176); Fax: +962-(0)6-534-8932



**Citation:** Ghazzy, A.; Taher, D.; Korb, M.; Al Khalyfeh, K.; Helal, W.; Amarne, H.; Rüffer, T.; Ishtaiwi, Z.; Lang, H. Rearrangement of Diferrocenyl 3,4-Thiophene Dicarboxylate. *Inorganics* **2022**, *10*, 96. <https://doi.org/10.3390/inorganics10070096>

Academic Editors: Duncan H. Gregory, Torben R. Jensen, Claudio Pettinari, Vladimir Arion, Wolfgang Linert and Richard Dronskowski

Received: 23 May 2022

Accepted: 22 June 2022

Published: 6 July 2022

**Publisher's Note:** MDPI stays neutral with regard to jurisdictional claims in published maps and institutional affiliations.



**Copyright:** © 2022 by the authors. Licensee MDPI, Basel, Switzerland. This article is an open access article distributed under the terms and conditions of the Creative Commons Attribution (CC BY) license (<https://creativecommons.org/licenses/by/4.0/>).

**Abstract:** Treatment of 3,4-(ClC(O))<sub>2</sub>-<sup>c</sup>C<sub>4</sub>H<sub>2</sub>S (**1**) with [FcCH<sub>2</sub>OLi] (**2-Li**) (Fc = Fe(η<sup>5</sup>-C<sub>5</sub>H<sub>5</sub>)(η<sup>5</sup>-C<sub>5</sub>H<sub>4</sub>)) in a 1:2 ratio gave 3,4-(FcCH<sub>2</sub>OC(O))<sub>2</sub>-<sup>c</sup>C<sub>4</sub>H<sub>2</sub>S (**3**). Compound **3** decomposes in solution during crystallization to produce FcCH<sub>2</sub>OH (**2**) along with 3,4-thiophenedicarboxylic anhydride (**4**). The cyclic voltammogram of **3** exhibits a reversible ferrocene-related redox couple ( $E_{1/2} = 108$  mV, vs. Cp<sub>2</sub>Fe/Cp<sub>2</sub>Fe<sup>+</sup>) using [N<sup>n</sup>Bu<sub>4</sub>] [B(C<sub>6</sub>F<sub>5</sub>)<sub>4</sub>] as the supporting electrolyte. DFT calculations reveal that the energy values of the LUMO orbitals of **3** (3,4-thiophene core) show 1 eV higher energies than that one of 2,5-(FcCH<sub>2</sub>OC(O))<sub>2</sub>-<sup>c</sup>C<sub>4</sub>H<sub>2</sub>S (**5**), both compounds' HOMO orbitals are close to each other. Compound **4** was characterized by single X-ray structure analysis. It forms a band-type structure based on intermolecular O1...S1 interactions being parallel to (110) and (1-10) in the solid state, while electrostatic C...O interactions between the C=O functionalities of adjacent molecules connect both 3D-networks. Hirshfeld surface analysis was used to gain more insight into the intermolecular interactions in **4**, the enrichment ratios (*E*) suggest that O...H, S...S, and O...C are the most favored intermolecular interactions, as shown by *E* values above 1.20. The relevance of the weak O...H, O...O, and O...C contacts in stabilizing the molecular structure of **4** was highlighted by the interaction energies between molecular pairs.

**Keywords:** heterocycle; electrochemistry; X-ray structure analysis; Hirshfeld surface analysis; DFT calculation

## 1. Introduction

Since ferrocene's discovery in 1951, its derivatives have played an increasingly essential role in chemistry during the following few decades [1–4]. Ferrocene-derived species were inspected broadly within the field of organometallic chemistry, e.g., as high-burning rate catalysts [5], as catalysts in homogeneous catalysis [6], as building blocks in model systems for molecular wires [7–14]. Or as active ingredients in anticancer therapies [15,16]. As a result, charge transfer interactions with ferrocenyl-functionalized -conjugated hydrocarbons, such as arenes or five- and six-membered heterocycles, have been investigated [17–21].

Multi-ferrocenyl compounds, particularly biferrrocene complexes in which two ferrocenyl units are connected by separate covalent units, can easily form mixed-valent (MV)

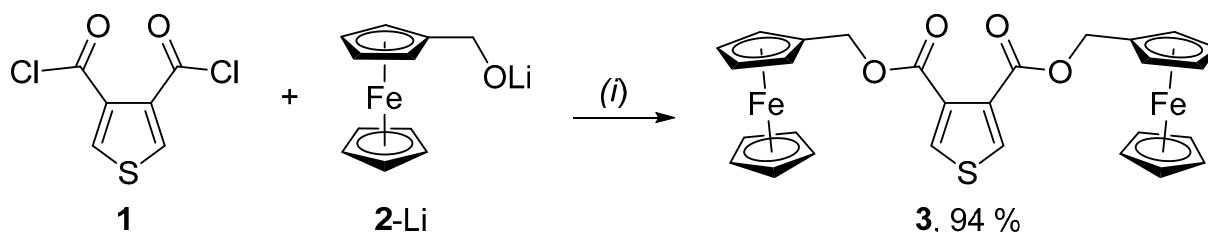
Fe(II)-Fe(III) species by chemical or electrochemical oxidation [22–24]. As electronic wires, these compounds have received attention lately [25,26]. In specific, Electrochemical studies of electronic intramolecular communication among covalently coupled redox units have made extensive use of such substances.

On the other hand, convenient and efficient synthetic methodologies of fused thiophenes has attracted considerable attention, due to the importance of such compounds as scaffolds in the world of pharmaceuticals and functional materials [27–31]. Fused thiophenes can be accessed by a variety of reactions [32–36] including the Rosenmund–von Braun reaction [37], intramolecular Friedel–Crafts acylations [38] and Suzuki–Miyaura carbon, carbon cross-couplings [39].

In order to continue our research on ferrocenyl-substituted compounds [40–52], this article reports on the reaction chemistry and chemical and physical properties of the ferrocenylmethylester 3,4-[Fe( $\eta^5$ -C<sub>5</sub>H<sub>5</sub>)( $\eta^5$ -C<sub>5</sub>H<sub>4</sub>CH<sub>2</sub>OC(O))<sub>2</sub>-<sup>c</sup>C<sub>4</sub>H<sub>2</sub>S (3). The formation of FcCH<sub>2</sub>OH (2) along with thieno [3,4-*c*]furan-1,3-dione (7) from 3 is discussed.

## 2. Results and Discussion

Treatment of diacid dichloride 3,4-(ClC(O))<sub>2</sub>-<sup>c</sup>C<sub>4</sub>H<sub>2</sub>S (1) with two equiv. of FcCH<sub>2</sub>OLi (2-Li) at –78 °C in diethyl ether gave 3,4-(FcCH<sub>2</sub>OC(O))<sub>2</sub>-<sup>c</sup>C<sub>4</sub>H<sub>2</sub>S (3) in excellent yield (Scheme 1, Experimental).



**Scheme 1.** Synthesis of 3. (i) 1 (1 equiv), 2-Li (2 equiv), diethyl ether, –78 °C, 18 h. Yield is based on 1. 2-Li was prepared in situ by an equimolar reaction of 2 with MeLi in diethyl ether [45,49].

The newly synthesized ferrocenyl-thiophene 3 did not require elaborative purification procedures. After diethyl ether filtration of the reaction mixture through a pad of Celite, followed by removal of all volatiles, the obtained residue was precipitated from a chloroform/hexane mixture of ratio 3:1 (*v/v*).

Compound 3 was identified by IR and <sup>1</sup>H and <sup>13</sup>C{<sup>1</sup>H} NMR spectroscopies, elemental analysis, high-resolution mass spectrometry, and electrochemistry.

The IR spectrum of a freshly purified sample of 3, for example, shows a characteristic  $\nu(\text{CO})$  stretching vibration at 1706 cm<sup>–1</sup>, typical for carbonyl functionalities of the C(O)OCH<sub>2</sub>Fc units [45,49,53].

The <sup>1</sup>H NMR spectrum of 3 is consistent with its molecular structure, showing resonance signals with the expected coupling patterns for the ferrocenyl groups and the heterocyclic moiety (Experimental) [40–42,44,48,49]. The ferrocenyl' C<sub>5</sub>H<sub>5</sub> protons of 3 give rise to a singlet at 4.17 ppm, while the ones of the C<sub>5</sub>H<sub>4</sub> rings appear as two pseudo-triplets at 4.32 and 4.20 ppm with *J*<sub>HH</sub> = 1.7 Hz, appearing in a similar range as characteristic for the analogous 2,5-substituted isomer 2,5-[(Fe( $\eta^5$ -C<sub>5</sub>H<sub>5</sub>)( $\eta^5$ -C<sub>5</sub>H<sub>4</sub>CH<sub>2</sub>OC(O))<sub>2</sub>-<sup>c</sup>C<sub>4</sub>H<sub>2</sub>S (5). [49,54] The <sup>c</sup>C<sub>5</sub>H<sub>2</sub>S and the CH<sub>2</sub> protons are observed as singlets at 7.79 and 5.04 ppm, respectively.

In the <sup>13</sup>C{<sup>1</sup>H} NMR spectrum of 3 the signal of the carbonyl carbon atom of the C(O)OCH<sub>2</sub>Fc entity, observed at 163.0 ppm, is the most representative [49]. The  $\alpha$  and  $\beta$  carbon atoms of the thiophene moiety appear at 131 and 133 ppm, respectively. All other organic groups show the anticipated signals without any peculiarities [49].

The electrochemical investigations of 3 were carried out under an atmosphere of argon in dichloromethane solutions containing [N<sup>+</sup>Bu<sub>4</sub>] [B(C<sub>6</sub>F<sub>5</sub>)<sub>4</sub>] (0.1 M) as supporting electrolyte at 25 °C and were referenced against the potential of the FcH/FcH<sup>+</sup> redox couple (Figure 1) [55].

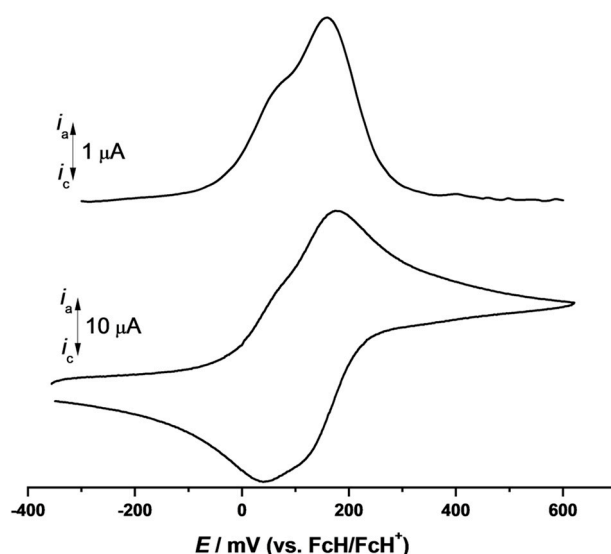


**Figure 1.** Cyclic voltammogram (bottom) and square-wave voltammogram (top) of **3** in anhydrous dichloromethane solutions (1.0 mM) at 25 °C, supporting electrolyte  $[N^nBu_4][B(C_6F_5)_4]$  (0.1 M), 100 mV/s.

From the cyclic voltammetry data, two individual reversible one-electron processes with  $i_{pc}/i_{pa}$  ratio close to unity are observed and the formal potentials (Figure 1,  $\Delta E^{o'}$  = 69 mV, and 146 mV, respectively) are significantly anodic shifted in comparison to the ferrocene redox event ( $Cp_2Fe/Cp_2Fe^+$ ) reflecting the electron-withdrawing nature of the  $-OC(O)R$  substituents. However, the presence of a small redox splitting between the first and the second oxidation step may indicate a certain degree of electronic and electrostatic interactions between the ferrocene moieties through the 3,4-dicarboxylate thiophene bridges [56,57]. Such behavior were noticed in a previously made electrochemical analysis of aryl-functionalized ferrocenylmethylesters (2,5- $[(Fe(\eta^5-C_5H_5)(\eta^5-C_5H_4CH_2OC(O)))_2-C_4H_2S]$ , (label as **5** with the corresponding literature)) [49]. In addition, in comparing, a difference in the electronic and the electrostatic interactions as a function to the relative position of the two ferrocenylmethyl-carboxylates on the thiophene ring are noticed too and reflected as the redox potentials of **3** significantly anodically shifted.

In order to observe the effect of the different substituents on the electronic properties of **3** and **5** the calculated energies and electron densities of the frontier molecular orbitals were investigated. Figure 2 summarizes the calculated energies of the HOMO and LUMO orbitals, in particular, the HOMO-LUMO energy gap values and the appropriate HOMO and LUMO contour plots of **3** and **5**.

The DFT results of **3** and **5** reveal that the lowest unoccupied molecular orbitals are localized on the heterocycle fragment with no contribution from the ferrocenyls. On the other hand, for **3** it is found that the HOMOs are localized on one ferrocenyl fragment, while for **8** they are localized on both ferrocenyls. The energy levels of the HOMO orbitals of both compounds are clearly close to each other, while the calculated LUMO orbitals of **3** show with 1 eV higher energies than that of **8**. The LUMO orbital energy increases significantly as a function of the relative positions of the two ferrocenylmethyls on the thiophene ring in **3** and **5**, indicating that changing the position of the fragments on the thiophene ring reduces electron density delocalization within the thiophene ring in the LUMO. A similar tendency was observed for the two  $FcCH_2$  units on the six membered aromatic ring  $[(FcCH_2OC(O))_2-C_6H_4]$ , by switching from *ortho* to *para* positions [49].

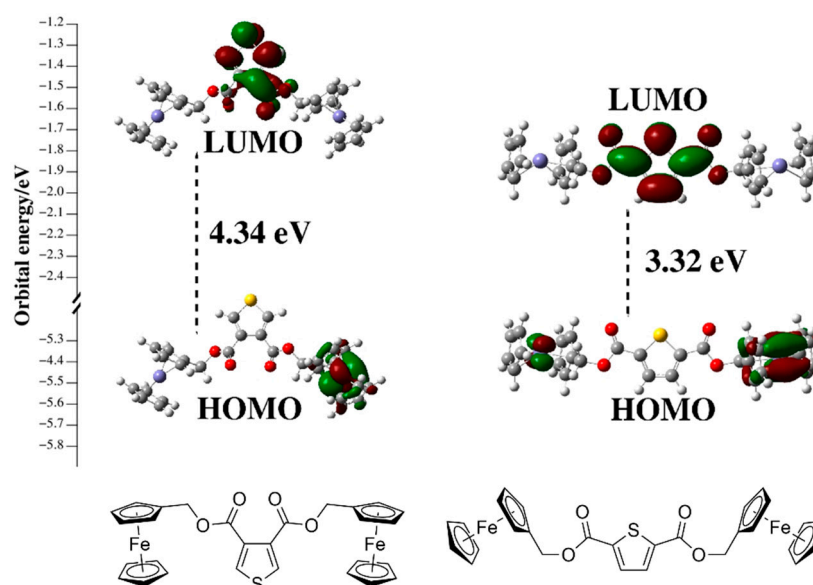
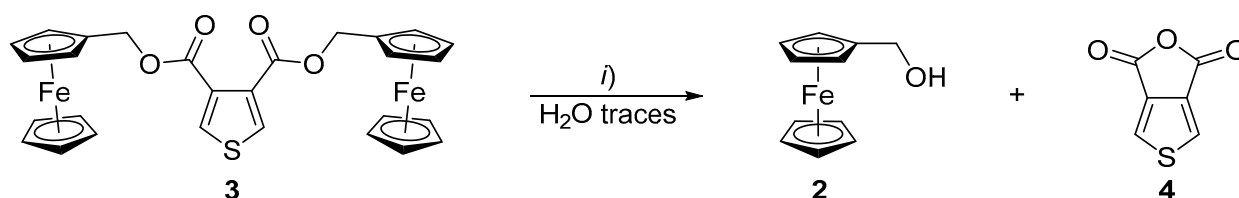


**Figure 2.** Frontier orbitals (HOMO and LUMO) for compounds **3** (left) and **5** (right), calculated at the B3LYP/6-31+G(d,p) and LANL2DZ level in dichloromethane, with isosurface 0.04. The HOMO-LUMO gap for both compounds is indicated in eV.

In attempts to grow single crystals of **3** in chloroform: hexane (ratio 1:4 *v/v*) solvent mixtures under air at  $-18\text{ }^{\circ}\text{C}$ , it was found that **3** further reacts with moisture and forms hydroxymethyl ferrocene (**2**) and 3,4-thiophenedicarboxylic anhydride (**4**) (Scheme 2). The structures of compounds **2** and **4** were identified based on their spectroscopy data and by comparison of their data with literature sources [37,58].



**Scheme 2.** Formation of thieno [3,4-*c*]furan-1,3-dione (**7**) by the  $\text{H}_2\text{O}$ -mediated cyclization of **3** under atmospheric conditions to give **2** and **4**.

The molecular structure of **4** in the solid state was determined by single crystal X-ray structure analysis. Pale yellow plates were obtained by cooling a chloroform/hexane mixture of ratio 1:4 (*v/v*) containing **4** to  $-18\text{ }^{\circ}\text{C}$ . Table S1 (See the ESI) summarizes the compound's crystallographic and refining data. Figure 3 depicts the molecular structure of **7**, with selected bond distances ( $\text{\AA}$ ), angles, and torsion angles ( $^{\circ}$ ) are listed in the caption.

Up to now, the crystal structures of fused thiophene compounds have been reported rarely. The title compound, thieno [3,4-*c*]furan-1,3-dione, with the molecule formula of  $\text{C}_6\text{H}_2\text{O}_3\text{S}$ , crystallizes in the tetragonal space group  $P 4_2/n$ . All of the atoms are nearly coplanar. The thiophene ring displays C–C single bond lengths of 1.407(3)  $\text{\AA}$ , slightly different to those in the furan ring (1.465(3) and 1.465(3)  $\text{\AA}$ ). The C=C double bond lengths are 1.356(3)/1.361(3)  $\text{\AA}$ . The C–O bond distances can clearly be distinguished between carbonyl C=O (1.191(3)  $\text{\AA}$  and 1.195(3)  $\text{\AA}$ ) and ether C–O (1.401(2)  $\text{\AA}$  and 1.405(2)  $\text{\AA}$ ). All bond lengths and angles of the fused thiophenes compound are normal and comparable with its analogues [14,40]. The molecular association pattern is dominated by  $\text{S}\cdots\text{O}$  and  $\text{O}\cdots\text{O}$  interactions found within the sum of van der Waals radii ( $\text{O/S} = 1.52, 1.8\text{ \AA}$ ,  $\Sigma = 3.32\text{ \AA}$ ;  $\text{O/O} = 1.52\text{ \AA}$ ,  $\Sigma = 3.02\text{ \AA}$ ). Most prominent is a square arrangement of four molecules of based on short  $\text{O}\cdots\text{O}$  distances between carbonyl oxygens O2 and O3 (Figure 4). Notably, the square interaction pattern is associated with short  $\text{O}\cdots\text{C}$  interactions based on O2 and

the adjacent anhydride ring in a *T*-shaped  $\pi$  fashion (omitted in Figure 4). The latter displays a very short distance between O2 and the centroid (Ct) of the heterocycle of 2.8292(4) Å ( $C2-O2\cdots Ct = 140.95(1)^\circ$ ), indicating a strong donor-acceptor interaction. Further short  $O\cdots C$  contacts appear between the  $C1=O1$  functionalities of two adjacent molecules, with the electron-rich oxygen being positioned over the carbonyl carbon ( $O1\cdots C1 = 3.1802(4)$  Å).

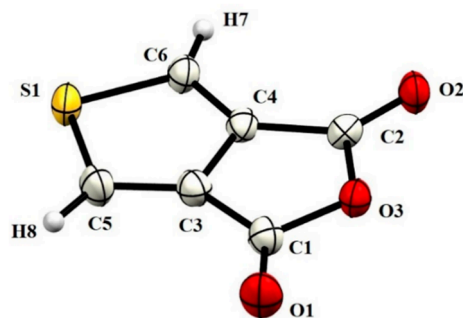


**Figure 3.** ORTEP (50% probability level) of the molecular structure of **4** with the atom-numbering scheme. Selected bond distances (Å), angles ( $^\circ$ ) and torsion angles ( $^\circ$ ): S1–C5 = 1.722(2), S1–C6 = 1.713(2), O1–C1 = 1.195(3), O3–C2 = 1.191(3), O2–C2 = 1.405(2), O3–C1 = 1.401(2), C1–C3 = 1.465(3), C2–C4 = 1.465(3), C3–C4 = 1.407(3), C4–C6 = 1.356(3), C3–C5 = 1.361(3); O1–C1–O3 = 119.68(18), O3–C1–C3 = 106.60(16), C2–O3–C1 = 110.65(15), C6–S1–C5 = 93.75(10), C1–C3–C4–C6 =  $-178.53(16)$ , O1–C1–O3–C2 = 178.62(19), C4–C6–S1–C5 =  $-0.25(15)$ .

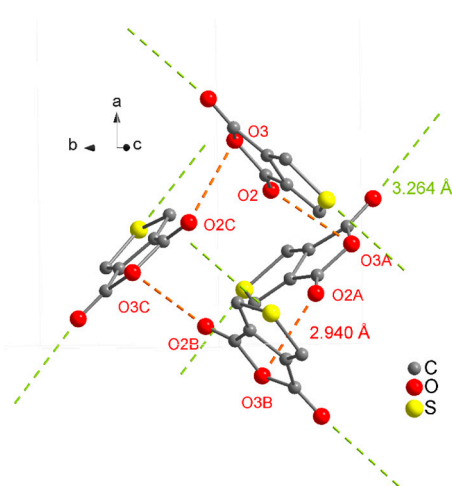


**Figure 4.** Intermolecular interactions within the sum of the van-der-Waals radii for compound **4**, showing the central square pattern. Symmetry operation for generating equivalent atoms: (A)  $y, 1/2 - x, 3/2 - z$ ; (B)  $1/2 - x, 1/2 - y, z$ ; (C)  $1/2 - y, x, 3/2 - z$ .

Via S1 and the O1-labeled carbonyl oxygen the cubic structure interacts further via  $O1\cdots S1$  contacts that are present at both sites of the molecules, forming a band-type structure (Figure 5). Based on the square arrangement these bands form planes parallel to (110) and (1–10) hence intersecting perpendicularly. Furthermore, weak intermolecular  $C-H\cdots O$  hydrogen bonding stabilizes the crystal packing of **7** (Table 1).

**Table 1.** Hydrogen bond geometry (Å,  $^\circ$ ) for compound **7**.

D–H $\cdots$ A	D–H	H $\cdots$ A	D $\cdots$ A	D–H $\cdots$ A
C6–H7 $\cdots$ O2 <sup>i</sup>	0.93	2.54	3.2708(4)	136
C6–H7 $\cdots$ O1 <sup>ii</sup>	0.93	2.57	3.1211(4)	118

Symmetry codes: (i)  $-1 + y, 1/2 - x, 1/2 - z$  (ii)  $-1/2 + x, -1/2 + y, -z$ .

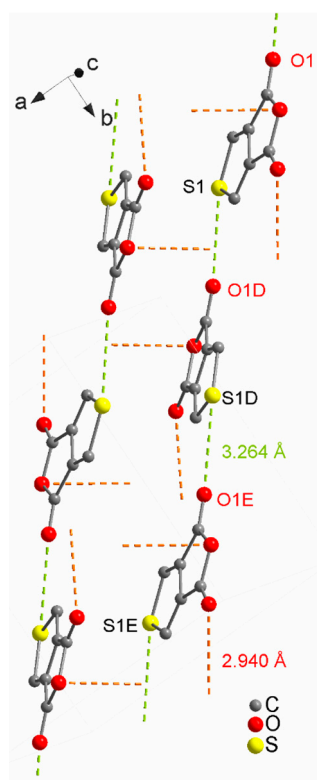


**Figure 5.** Intermolecular interaction in the packing of **7**, highlighting the O1...S1 pattern parallel to (1–10). Symmetry operation for generating equivalent atoms: (D)  $-1/2 + x, -1/2 + y, -z$ ; (E)  $x + 1, y - 1, z$ .

In total, a three-dimensional network is formed based on short and very strong interaction patterns. However, cavities remain (Figure 6, top), which are filled by an individual second network that interpenetrates the first one highlighted in black and blue in Figure 6. Weaker dispersion interactions between the  $\pi$ -orbitals of the C=O functionalities of adjacent molecules ( $O/C = 3.18 \text{ \AA}$ ;  $\sum_{O,x} = 3.22 \text{ \AA}$ ) connect both 3D-networks (Figure 7).

To accomplish the description of the supramolecular connectivity in the crystal structure of **1**, a Hirshfeld surface analysis was realized. Maps of the Hirshfeld surface, shape index and curvedness were generated based on the crystallographic information file (CIF) using the CrystalExplorer 3.1 program [59,60]. Hirshfeld surfaces enable the visualization of intermolecular interactions and indicate the relative strength of the interactions by different colors and color intensity. In the  $d_{\text{normal}}$  map (Figure 8), the vivid red spots are due to short normalized  $O\cdots H/H\cdots O$ ,  $C\cdots O/H\cdots C$ ,  $O\cdots S/S\cdots O$ ,  $O\cdots O$ ;  $C\cdots C$ ,  $H\cdots H$ ,  $S\cdots S$ , and  $C\cdots H$  interactions. The white areas depicted at either side of the molecular structures in the Hirshfeld surface represent the aromatic rings and are footmarks of pep interactions [61,62]. On the shape-index surface of compound **4**, convex blue regions represent hydrogen-donor groups and concave red regions represent hydrogen-acceptor groups. Figure 8 illustrates that the thiophene unit behaves simultaneously as donor and acceptor group. Meanwhile, the carbonyl substituents are acceptors only. Two-dimensional fingerprint plots quantify the contributions of each type of non-covalent interactions on the Hirshfeld surface map [63,64]. Analysis of the 2D fingerprint plots (Figure 9) reveals that the major contribution corresponding to 39.8% of the surface is due to  $O\cdots H/H\cdots O$  contacts (Figure 9f), indicating that aside from hydrogen bonding interactions van der Waals contacts are relevant for the molecular packing in the crystal structure.  $C\cdots O/H\cdots C$  interactions contribute 18.2% (Figure 8g), the  $O\cdots S/S\cdots O$  interactions 9.9% (Figure 9h), while  $O\cdots O$  contributes 6.2% (Figure 9c). The remaining contacts, i.e.,  $C\cdots C$ ,  $H\cdots H$ ,  $S\cdots S$  and  $C\cdots H$ , respectively, to the crystal structure stabilization (Figure 9a,b,d,e).

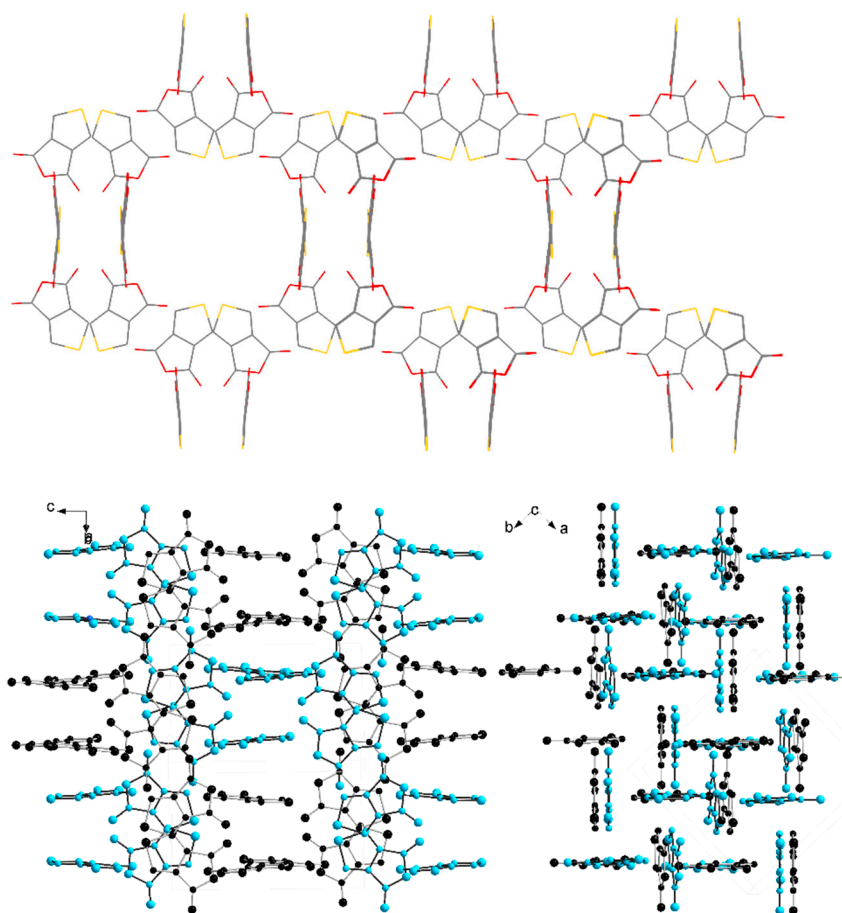


**Figure 6.** Combination of the interaction pattern of **4**, described in Figures 4 and 5 (top), and two interpenetrating networks of strong O...S interactions that complete the packing in the solid state of **4**.

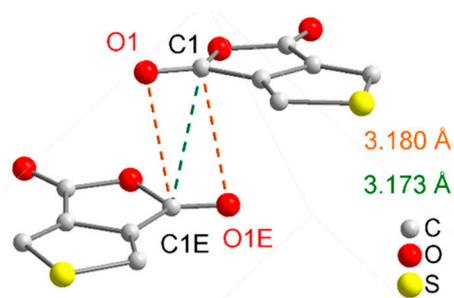


**Figure 7.** Electrostatic C...O interactions of **7**, that occur between both interpenetrating networks, shown in Figure 6.

The enrichment ratios  $E$ , the ratio between the actual contacts proportion in the crystal and random contacts (theoretical proportion), were computed with MoProViewer program [65]. Values of  $E > 1$  indicate that the pair of elements involved have a high propensity to form contacts in the crystal structure, while an  $E < 1$  value indicates that the propensity would be low [66]. The contributions to the surfaces (taking into account the inner and outer surfaces) in **4** and the corresponding enrichment ratios are presented in Table 2. The enrichment ratios of **4** show that the O...H contacts ( $E_{OH} = 2.18$ ) is the most favoured contact in the crystal packing followed by the S...S ( $E_{SS} = 2.04$ ), O...C ( $E_{OC} = 1.21$ ) and C...C contacts ( $E_{CC} = 1.16$ ), respectively. The O...H contacts cover 24.98% of the total Hirshfeld surface of **4**, while the surface contacts of O...C covers 22.97%, illustrating the importance of these relatively weak interactions in the molecular packing of **4**.

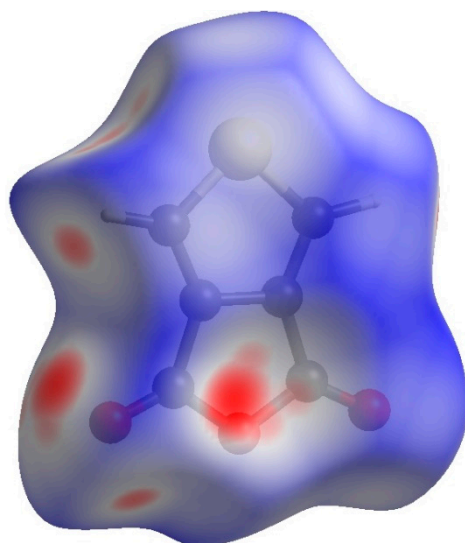


Figure 8. Hirshfeld surface of compound 4.

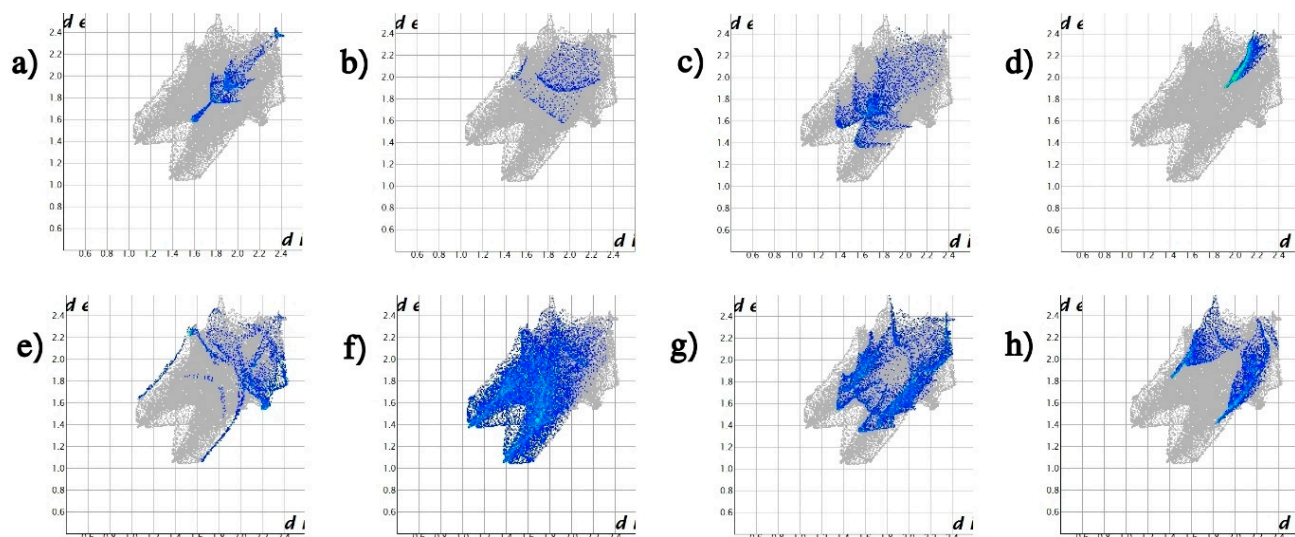


Figure 9. Hirshfeld fingerprint plots of compound 4 for (a) C...C, (b) H...H interactions, (c) O...O, (d) S...S, (e) C-H/H-C, (f) O-H/H-O, (g) C...O/O...C and (h) O...S/S...O interactions.

Interaction energies were computed using CrystalExplorer to evaluate the role of the various intermolecular interactions in stabilizing the molecular packing of 4 [67]. The interaction energies between molecular pairs were calculated for a cluster of 3.8 Å around the central molecule. The molecular pair interaction energies are expressed in terms of total energy ( $E_{tot}$ ), electrostatic energy ( $E_{ele}$ ), polarization energy ( $E_{pol}$ ), dispersion energy ( $E_{dis}$ ), and repulsion energy ( $E_{rep}$ ). The values of these energies for 4 are listed in Table 3. The highest stabilized molecular pairs in 4 ( $E = -32.5$  kJ/mol) is related to the three molecules linked by the O...O, O...H and O...C short contacts (all within the sum of van der Waals radii), where the main stabilizing energy is due to the  $E_{ele}$  contribution followed by  $E_{dis}$ . The second highest stabilized molecular pairs in 4 ( $E = -16.1$  kJ/mol) are related to the three molecules linked by the S...O, O...H and O...C short contacts (all within the sum of van der Waals radii). The main stabilizing energy of these molecules is also due to the  $E_{ele}$  contribution followed by  $E_{dis}$ .

**Table 2.** Hirshfeld contact surfaces and enhancement ratios (*E*) for **4**.

Atoms	H	C	O	S
Surface interior (%)	17.53	30.67	31.41	20.39
Surface exterior (%)	17.86	28.16	33.22	20.76
Actual contacts merged (%)				
H	0.68	-	-	-
C	6.37	10.00	-	-
O	24.98	22.97	2.50	-
S	2.68	9.48	11.69	8.65
Equiprobable contacts merged (%)				
H	3.13	-	-	-
C	10.41	8.64	-	-
O	11.43	19.03	10.43	-
S	7.28	12.11	13.30	4.23
Enrichment reciprocal contacts merged (%)				
H	0.22	-	-	-
C	0.61	1.16	-	-
O	2.18	1.21	0.24	-
S	0.37	0.78	0.88	2.04

**Table 3.** Selected interaction energies (kJ/mol) (with  $E_{\text{tot}} > -50.0$  kJ/mol) for **4**.

Contacts	Symmetry Operation	$E_{\text{ele}}$	$E_{\text{pol}}$	$E_{\text{dis}}$	$E_{\text{rep}}$	$E_{\text{tot}}$
O...O, O...H, and O...C	$y, -x + 1/2, -z + 1/2$	-25.7	-5.0	-17.6	22.2	-32.5
S...O, O...H, and O...C	$x + 1/2, y + 1/2, -z$	-13.4	-2.8	-6.6	9.5	-16.1

### 3. Conclusions

The synthesis of 3,4-((FcCH<sub>2</sub>OC(O))<sub>2</sub>)<sub>2</sub>-C<sub>4</sub>H<sub>2</sub>S (**3**) by treatment of FcCH<sub>2</sub>OLi with 3,4-(ClC(O))<sub>2</sub>-C<sub>4</sub>H<sub>2</sub>S (**2**) is described. Electrochemical measurements on **3** showed that the substitution pattern of the ester on the aryl ring and the electron-withdrawing effect of the acyl groups influences the electrochemical shift of the formal potential. The respective aryl system possesses a significantly higher Fc/Fc<sup>+</sup> vs. Cp<sub>2</sub>Fe/Cp<sub>2</sub>Fe<sup>+</sup> redox potential as observed for the more electron-rich ferrocenemethanol [68,69]. DFT calculations show different degrees of HOMO-LUMO energy gaps when comparing **3** with **5** due to changing the LUMO energy depending on the positions of the carboxylic ester substituents on the thiophene rings. Compound **3** decomposes in solution with moisture to form 1-hydroxymethyl ferrocene (**2**) and thieno [3,4-*c*]furan-1,3-dione (**4**) which was characterized by single X-ray structure analysis.

**Supplementary Materials:** The following supporting information can be downloaded at: <https://www.mdpi.com/article/10.3390/inorganics10070096/s1>, Table S1: Crystallographic data and refinement details for **4**.

**Author Contributions:** Investigation A.G.; Conceptualization, Writing—original draft, D.T.; Conceptualization, Single Crystal data collection and analysis, M.K. And T.R.; Formal analysis, K.A.K., W.H., H.A. and Z.I.; Funding acquisition, H.L. All authors have read and agreed to the published version of the manuscript.

**Funding:** We are grateful to the University of Jordan and Al Ahliyya Amman University for financial support.

**Institutional Review Board Statement:** Not applicable.

**Informed Consent Statement:** Not applicable.

**Data Availability Statement:** Not applicable.

**Acknowledgments:** The authors greatly appreciate and acknowledge of financial support received from the University of Jordan and Al Ahliyya Amman University.

**Conflicts of Interest:** The authors declare no conflict of interest.

**Supporting Data:** Crystallographic data (excluding structure factors) have been deposited with the Cambridge Crystallographic Data Centre as supplementary publication CCDC-2099570 for 4. Copies of the data can be obtained free of charge on application to CCDC, 12 Union Road, Cambridge CB2 1EZ, UK [E-mail: deposit@ccdc.cam.ac.uk].

## References

1. Kealy, T.J.; Pauson, P.L. A new type of organo-iron compound. *Nature* **1951**, *168*, 1039. [[CrossRef](#)]
2. Miller, S.A.; Tebboth, J.A.; Tremaine, J.F. Dicyclopentadienyliron. *J. Chem. Soc.* **1952**, *114*, 632. [[CrossRef](#)]
3. Van Staveren, D.R.; Metzler-Nolte, N. Bioorganometallic chemistry of ferrocene. *Chem. Rev.* **2004**, *104*, 5931. [[CrossRef](#)] [[PubMed](#)]
4. Štěpnička, P. (Ed.) *Ferrocenes: Ligands, Materials and Biomolecules*; Wiley & Sons: Chichester, UK, 2008.
5. Tong, R.; Zhao, Y.; Wang, L.; Yu, H.; Ren, F.; Saleem, M.; Amer, W.A. Recent research progress in the synthesis and properties of burning rate catalysts based on ferrocene-containing polymers and derivatives. *J. Organomet. Chem.* **2014**, *755*, 16. [[CrossRef](#)]
6. Dai, L.-X.; Hou, X.-L. (Eds.) *Chiral Ferrocenes in Asymmetric Catalysis; Synthesis and Applications*; Wiley-VCH: Weinheim, Germany, 2010.
7. Yu, Y.; Bond, A.D.; Leonard, P.W.; Lorenz, U.J.; Timofeeva, T.V.; Vollhardt, K.P.C.; Whitener, G.D.; Yakovenko, A.A. Hexaferrocenylbenzene. *Chem. Commun.* **2006**, *24*, 2572. [[CrossRef](#)]
8. Yu, Y.; Bond, A.D.; Leonard, P.W.; Vollhardt, K.P.C.; Whitener, G.D. Syntheses, structures, and reactivity of radial oligocyclopentadienyl metal complexes: Penta (ferrocenyl) cyclopentadienyl and congeners. *Angew. Chem. Int. Ed.* **2006**, *45*, 1794. [[CrossRef](#)]
9. Hildebrandt, A.; Rüffer, T.; Erasmus, E.; Swarts, J.C.; Lang, H. A star-shaped supercrowded 2,3,4,5-tetraferrocenylthiophene: Synthesis, solid-state structure, and electrochemistry. *Organometallics* **2010**, *29*, 4900–4905. [[CrossRef](#)]
10. Frenzel, P.; Lehigh, S.W.; Korb, M.; Hildebrandt, A.; Lang, H. Ferrocenyloxysilanes: Synthesis, characterization and electrochemical investigations. *J. Organomet. Chem.* **2017**, *845*, 98. [[CrossRef](#)]
11. Packheiser, R.; Lang, H. Mixed transition–metal complexes based on multitopic 1,3,5-triethynyl-and 1-diphenylphosphino-3,5-diethynyl-benzene linking units. *Inorg. Chim. Acta* **2011**, *366*, 177–183. [[CrossRef](#)]
12. Packheiser, R.; Rüffer, T.; Ecorchard, P.; Lang, H.Z. Transition-Metal Complexes Based on the 1,3,5-Triethynyl Benzene Linking Unit. *Anorg. Allg. Chem.* **2010**, *636*, 2607. [[CrossRef](#)]
13. Packheiser, R.; Lang, H. A first mixed heteropentametall transition metal complex: Synthesis and characterisation. *Chem. Commun.* **2007**, *10*, 580. [[CrossRef](#)]
14. Barlow, S.; O'Hare, D. Metal–metal interactions in linked metallocenes. *Chem. Rev.* **1997**, *97*, 637. [[CrossRef](#)] [[PubMed](#)]
15. Paul, F.; Lapinte, C. Organometallic molecular wires and other nanoscale-sized devices: An approach using the organoiron (dppe) Cp\* Fe building block. *Coord. Chem. Rev.* **1998**, *178–180*, 431–509. [[CrossRef](#)]
16. Lal, B.; Badshah, A.; Altaf, A.A.; Khan, N.; Ullah, S. Miscellaneous applications of ferrocene-based peptides/amides. *Appl. Organomet. Chem.* **2011**, *25*, 843. [[CrossRef](#)]
17. Braga, S.S.; Silva, A.M.S. A new age for iron: Antitumoral ferrocenes. *Organometallics* **2013**, *32*, 5626. [[CrossRef](#)]
18. Hildebrandt, A.; Lang, H. (Multi) ferrocenyl five-membered heterocycles: Excellent connecting units for electron transfer studies. *Organometallics* **2013**, *32*, 5640. [[CrossRef](#)]
19. Ceccon, A.; Santi, S.; Orian, L.; Bisello, A. Electronic communication in heterobinuclear organometallic complexes through unsaturated hydrocarbon bridges. *Coord. Chem. Rev.* **2004**, *248*, 683. [[CrossRef](#)]
20. Ward, M.D. Metal-metal interactions in binuclear complexes exhibiting mixed valency; molecular wires and switches. *Chem. Soc. Rev.* **1995**, *24*, 121. [[CrossRef](#)]
21. Hildebrandt, A.; Lang, H. Influencing the electronic interaction in diferrocenyl-1-phenyl-1 H-pyrroles. *Dalt. Trans.* **2011**, *40*, 11831. [[CrossRef](#)]
22. Li, Y.; Josowicz, M.; Tolbert, L.M. Diferrocenyl molecular wires. The role of heteroatom linkers. *J. Am. Chem. Soc.* **2010**, *132*, 10374. [[CrossRef](#)]
23. Moriuchi, T.; Hirao, T. Imide-bridged diferrocene for protonation-controlled regulation of electronic communication. *Tetrahedron Lett.* **2007**, *48*, 5099. [[CrossRef](#)]

24. Guldi, D.M.; Maggini, M.; Scorrano, G.; Prato, M. Intramolecular electron transfer in fullerene/ferrocene based donor–bridge–acceptor dyads. *J. Am. Chem. Soc.* **1997**, *119*, 974. [[CrossRef](#)]
25. Sixt, T.; Sieger, M.; Krafft, M.J.; Bubrin, D.; Fiedler, J.; Kaim, W. Ambi-valence taken literally: Ruthenium vs iron oxidation in (1,1'-diphosphinoferrocene) ruthenium (II) hydride and chloride complexes as deduced from spectroelectrochemistry of the heterodimetallic “mixed-valent” intermediates. *Organometallics* **2010**, *29*, 5511. [[CrossRef](#)]
26. Nguyen, P.; Elipe, P.G.; Manners, I. Organometallic polymers with transition metals in the main chain. *Chem. Rev.* **1999**, *99*, 1515. [[CrossRef](#)] [[PubMed](#)]
27. MacDowell, D.W.H.; Jourdenais, R.A.; Naylor, R.W.; Wisowaty, J.C. The Reaction of Thiophene-3,4-dicarbonyl Chloride with Aluminum Chloride and Benzene. *J. Org. Chem.* **1972**, *37*, 4406. [[CrossRef](#)]
28. El-Gaby, M.S.A.; Zahran, M.A.; Ismail, M.M.F.; Ammar, Y.A. A novel synthesis of dibenzo [c,f] chromenes, dibenzo [c,h] chromenes and benzo [7,8] chromeno [3,4-f] isoindoles as antimicrobial agents. *II Farmaco.* **2000**, *55*, 227.
29. Meyer, C.; Neue, B.; Schepmann, D.; Yanagisawa, S.; Yamaguchi, J.; Würthwein, E.-U.; Itami, K.; Wünsch, B. Exploitation of an additional hydrophobic pocket of  $\sigma$  1 receptors: Late-stage diverse modifications of spirocyclic thiophenes by C–H bond functionalization. *Org. Biomol. Chem.* **2011**, *9*, 8016. [[CrossRef](#)] [[PubMed](#)]
30. Meyer, C.; Schepmann, D.; Yanagisawa, S.; Yamaguchi, J.; Itami, K.; Wünsch, B. Late-Stage C–H Bond Arylation of Spirocyclic  $\sigma$ 1 Ligands for Analysis of Complementary  $\sigma$ 1 Receptor Surface. *Eur. J. Org. Chem.* **2012**, *2012*, 5972. [[CrossRef](#)]
31. Meyer, C.; Schepmann, D.; Yanagisawa, S.; Yamaguchi, J.; Col, V.D.; Laurini, E.; Itami, K.; Pricl, S.; Wünsch, B.J. Pd-catalyzed direct C–H bond functionalization of spirocyclic  $\sigma$ 1 ligands: Generation of a pharmacophore model and analysis of the reverse binding mode by docking into a 3D homology model of the  $\sigma$ 1 receptor. *Med. Chem.* **2012**, *55*, 8047. [[CrossRef](#)] [[PubMed](#)]
32. Meyer, C.; Neue, B.; Schepmann, D.; Yanagisawa, S.; Yamaguchi, J.; Würthwein, E.-U.; Itami, K.; Wünsch, B. Improvement of  $\sigma$ 1 receptor affinity by late-stage C–H-bond arylation of spirocyclic lactones. *Bioorg. Med. Chem.* **2013**, *21*, 1844. [[CrossRef](#)]
33. Al-Mousawi, S.M.; El-Asasery, M.A. Synthesis of some monoazo disperse dyes derived from aminothienchromene. *Molecules* **2013**, *18*, 8837. [[CrossRef](#)]
34. Fuse, S.; Takahashi, R.; Takahashi, T. Facile, One-Step Synthesis of 5-Substituted Thieno [3,4-c] pyrrole-4,6-dione by Palladium-Catalyzed Carbonylative Amidation. *Eur. J. Org. Chem.* **2015**, *16*, 3430. [[CrossRef](#)]
35. Kim, J.E.; Lee, J.; Yun, H.; Baek, Y.; Lee, P.H. Rhodium-catalyzed intramolecular transannulation reaction of alkynyl thiadiazole enabled 5, n-fused thiophenes. *J. Org. Chem.* **2017**, *82*, 1437–1447. [[CrossRef](#)] [[PubMed](#)]
36. Benachenhou, F.; Mesli, M.A.; El Borai, M.; Hanquet, B.; Guillard, R.J. Synthesis and structure elucidation of the condensation products between thiophene dicarbonyldehydes and aromatic amines. Potential analgesic and anti-inflammatory agents. *Heterocycl. Chem.* **1988**, *25*, 1531. [[CrossRef](#)]
37. Nielsen, C.B.; Bjørnholm, T. New regiosymmetrical dioxopyrrolo- and dihydropyrrolo-functionalized polythiophenes. *Org. Lett.* **2004**, *6*, 3381. [[CrossRef](#)] [[PubMed](#)]
38. Crayston, J.A.; Iraqi, A.; Mallon, P.; Walton, J.C. Preparation and characterisation of thienonaphthoquinones and their radical ions. *J. Chem. Soc. Perkin Trans.* **1993**, *2*, 1589. [[CrossRef](#)]
39. Vishnumurthy, K.; Makriyannis, A.J. Novel and Efficient One-Step Parallel Synthesis of Dibenzopyranones via Suzuki–Miyaura Cross Coupling. *Comb. Chem.* **2010**, *12*, 664. [[CrossRef](#)]
40. Taher, D.; Awwadi, F.F.; Pfaff, U.; Speck, J.M.; Rüffer, T.; Lang, H. A series of Se-ferrocenyl thiophene carboselenoates—Synthesis, solid-state structure and electrochemistry. *J. Organomet. Chem.* **2013**, *736*, 9. [[CrossRef](#)]
41. Taher, D.; Awwadi, F.F.; Speck, J.M.; Korb, M.; Schaarschmidt, D.; Weheabby, S.; Habashneh, A.Y.; Al-Noaimi, M.; El-Khateeb, M.; Abu-Orabi, S.T.; et al. Heterocyclic-based ferrocenyl carboselenolates: Synthesis, solid-state structure and electrochemical investigations. *J. Organomet. Chem.* **2017**, *845*, 55. [[CrossRef](#)]
42. Taher, D.; Awwadi, F.F.; Speck, J.M.; Korb, M.; Wagner, C.; Hamed, E.M.; Al-Noaimi, M.; Habashneh, A.Y.; El-khateeb, M.; Abu-Orabi, S.T.; et al. Ferrocenyl thiocarboxylates: Synthesis, solid-state structure and electrochemical investigations. *J. Organomet. Chem.* **2017**, *847*, 59. [[CrossRef](#)]
43. Taher, D.; Awwadi, F.F.; Speck, J.M.; Korb, M.; Schaarschmidt, D.; Wagner, C.; Amarné, H.; Merzweiler, K.; van Koten, G.; Lang, H.J. From ferrocenyl selenoesters to diferrocenyl methanols. *Organomet. Chem.* **2018**, *863*, 1. [[CrossRef](#)]
44. Taher, D.; Corrigan, J.F. Aryl (trimethylsilyl) selenides as Reagents for the Synthesis of Mono- and Diselenoesters. *Organometallics* **2011**, *30*, 5943. [[CrossRef](#)]
45. Ghazzy, A.; Taher, D.; Helal, W.; Korb, M.; Al-Shewikib, R.K.; Weheabby, S.; Al-Said, N.; Abu-Orabi, S.T.; Lang, H. Aryl ferrocenylmethylesters: Synthesis, solid-state structure and electrochemical investigations. *Arab. J. Chem.* **2020**, *13*, 3546. [[CrossRef](#)]
46. Taher, D. Synthesis and reactivity of cyclopentadienyl ruthenium complexes containing ferrocenylselenolates. *Transit. Met. Chem.* **2009**, *34*, 641. [[CrossRef](#)]
47. Taher, D.; Wallbank, A.I.; Turner, E.A.; Cuthbert, H.L.; Corrigan, J.F. Alk-2-ynyl Trimethylsilyl Chalcogenoethers by Nucleophilic Substitution of Propargyl Bromides. *Eur. J. Inorg. Chem.* **2006**, *22*, 4616. [[CrossRef](#)]
48. Taher, D.; Awwadi, F.; El-khateeb, M.; Lang, H. Synthesis and reactivity of cyclopentadienyl iron complexes containing ferrocenyl selenolates. *Transit. Met. Chem.* **2012**, *37*, 601. [[CrossRef](#)]

49. Taher, D.; Ghazzy, A.; Awwadi, F.F.; Helal, W.; al Khalyfeh, K.; Korb, M.; Hildebrandt, A.; Kovalski, E.; Lang, H. Ferrocenylmethyl-functionalized 5-membered heterocycles: Synthesis, solid-state structure and electrochemical investigations. *Polyhedron* **2018**, *152*, 188. [[CrossRef](#)]
50. Hildebrandt, A.; Miesel, D.; Lang, H. Electrostatic interactions within mixed-valent compounds. *Coord. Chem. Rev.* **2018**, *371*, 56. [[CrossRef](#)]
51. Lang, H. Organometallic  $\pi$ -tweezers and 1,1'-bis (diphenylphosphanyl) ferrocene as bidentate chelating ligands for the synthesis of heteromultimetallic compounds. *Polyhedron* **2018**, *139*, 50. [[CrossRef](#)]
52. Heinze, K.; Lang, H. Ferrocene—Beauty and Function. *Organometallics* **2013**, *20*, 5623. [[CrossRef](#)]
53. Naik, V.S.; Pragasam, A.; Jayanna, H.S.; Vinitha, G. Structural, linear optical, second and third-order nonlinear optical properties of two halogenated chalcone derivatives containing thiophene moiety. *Chem. Phys. Lett.* **2020**, *761*, 138051. [[CrossRef](#)]
54. Terpstra, J.W.; van Leusen, A.M. A new synthesis of benzo [b] thiophenes and benzo [c] thiophenes by annulation of disubstituted thiophenes. *J. Org. Chem.* **1986**, *51*, 230–238. [[CrossRef](#)]
55. Swarts, J.C.; Nafady, A.; Roudebush, J.H.; Trupia, S.; Geiger, W.E. One-electron oxidation of ruthenocene: Reactions of the ruthenocenium ion in gentle electrolyte media. *Inorg. Chem.* **2009**, *48*, 2156. [[CrossRef](#)] [[PubMed](#)]
56. Huang, P.; Jin, B.; Liu, P.; Cheng, L.; Cheng, W.; Zhang, S. Synthesis, electrochemistry and IR spectroelectrochemistry of bisferrocenyl bridged benzene derivatives. *J. Organomet. Chem.* **2012**, *697*, 57. [[CrossRef](#)]
57. Hildebrandt, A.; al Khalyfeh, K.; Nawroth, J.F.; Jordan, R. Electron transfer studies on conjugated ferrocenyl-containing oligomers. *Organometallics* **2016**, *35*, 3713. [[CrossRef](#)]
58. Kalita, D.; Morisue, M.; Kobuke, Y. Synthesis and electrochemical properties of slipped-cofacial porphyrin dimers of ferrocene-functionalized Zn-imidazolyl-porphyrins as potential terminal electron donors in photosynthetic models. *New J. Chem.* **2006**, *30*, 77. [[CrossRef](#)]
59. Hirshfeld, F.L. Bonded-atom fragments for describing molecular charge densities. *Theor. Chim. Acta* **1977**, *44*, 129–138. [[CrossRef](#)]
60. McKinnon, J.J.; Spackman, M.A.; Mitchell, A.S. Novel tools for visualizing and exploring intermolecular interactions in molecular crystals. *Acta Crystallogr. B* **2004**, *60*, 627–668. [[CrossRef](#)]
61. Spackman, M.A.; McKinnon, J.J. Fingerprinting intermolecular interactions in molecular crystals. *Cryst. Eng. Comm.* **2002**, *4*, 378–392. [[CrossRef](#)]
62. Liu, X.; Du, L.; Zhang, W.; Li, R.; Feng, F.; Feng, X.J. Syntheses, structures and hirshfeld surface analyses of two 3D supramolecules based on nitrogen-heterocyclic tricarboxylate ligand. *Mol. Struct.* **2019**, *1194*, 138–143. [[CrossRef](#)]
63. Gritzner, G.; Kuta, J. Recommendations on reporting electrode potentials in nonaqueous solvents. *Pure Appl. Chem.* **1984**, *56*, 461. [[CrossRef](#)]
64. Nafady, A.; Geiger, W.E. Characterization of the successive one-electron oxidation products of the dicobalt fulvalenediyl (Fv) compound Co<sub>2</sub>Fv (CO)<sub>4</sub> and its phosphine-substituted product. *Organometallics* **2008**, *27*, 5624. [[CrossRef](#)]
65. Guillot, B.; Enrique, E.; Huder, L.; Jelsch, C. MS19. O01. *Acta Cryst. A* **2014**, *70*, C279. [[CrossRef](#)]
66. Jelsch, C.; Ejsmont, K.; Huder, L. The enrichment ratio of atomic contacts in crystals, an indicator derived from the Hirshfeld surface analysis. *IUCr* **2014**, *1*, 119. [[CrossRef](#)] [[PubMed](#)]
67. Tan, S.L.; Jotani, M.M.; Tiekink, E.R.T. Utilizing Hirshfeld surface calculations, non-covalent interaction (NCI) plots and the calculation of interaction energies in the analysis of molecular packing. *Acta Crystallogr. E* **2019**, *75*, 308. [[CrossRef](#)] [[PubMed](#)]
68. Claus, R.; Lewtak, J.P.; Müller, T.J.; Swarts, J.C. Structural influences on the electrochemistry of 1, 1'-di (hydroxyalkyl) ferrocenes. Structure of [Fe ( $\eta^5$ -C<sub>5</sub>H<sub>4</sub>-CH (OH)-(CH<sub>2</sub>)<sub>3</sub>OH) <sub>2</sub>]. *J. Organomet. Chem.* **2013**, *740*, 61. [[CrossRef](#)]
69. Braga, D.; Maini, L.; Paganelli, F.; Tagliavini, E.; Casolari, S.; Grepioni, F.J. Organometallic building blocks for crystal engineering. Synthesis, structure and hydrogen bonding interactions in [Fe ( $\eta^5$ -C<sub>5</sub>H<sub>4</sub>-CH<sub>2</sub> (CH<sub>3</sub>) OH) <sub>2</sub>], [Fe ( $\eta^5$ -C<sub>5</sub>H<sub>3</sub> (CH<sub>3</sub>) COOH) <sub>2</sub>], [Fe ( $\eta^5$ -C<sub>5</sub>H<sub>4</sub>CH (CH<sub>3</sub>) NH ( $\eta^5$ -C<sub>5</sub>H<sub>4</sub>CH (CH<sub>3</sub>)))] and in the diaminecyclohexane salt [Fe ( $\eta^5$ -C<sub>5</sub>H<sub>4</sub>COO) <sub>2</sub>] <sub>2</sub> - [(1S, 2S)-(NH<sub>3</sub>)<sub>2</sub>C<sub>6</sub>H<sub>10</sub>] <sub>2</sub> + 2 [H<sub>2</sub>O]. *Organomet. Chem.* **2001**, *609*, 637–639.